Chemical Geology 479 (2018) 1–9

Contents lists available at ScienceDirect

Chemical Geology

journal homepage: www.elsevier.com/locate/chemgeo

Silicon isotopic compositions of altered oceanic crust: Implications for Si isotope heterogeneity in the mantle

Hui-Min Yu[a,*], Yuan-Hong Li[a], Yong-Jun Gao[b], Jian Huang[a], Fang Huang[a,*]

[a] CAS Key Laboratory of Crust-Mantle Materials and Environments, School of Earth and Space Sciences, University of Science and Technology of China, Hefei 230026, China

[b] Department of Earth and Atmospheric Sciences, University of Houston, Houston, TX 77204, USA

ARTICLE INFO

Editor: Catherine Chauvel

Keywords:
Silicon isotopes
Altered oceanic crust
Mantle
Subduction

ABSTRACT

This study reports Si isotope compositions of the altered oceanic crust recovered from IODP Site 1256, East Pacific Rise to investigate the behavior of Si isotopes during low-temperature seawater and/or high-temperature hydrothermal alteration processes in the oceanic crust. These samples, including basalts and gabbros, were altered by seawater and hydrothermal fluids at various temperatures and water/rock ratios. The $\delta^{30}Si$ of these samples range from $-0.38‰$ to $-0.27‰$, with an average of $\delta^{30}Si = -0.32 \pm 0.06‰$ (2SD, $N = 50$), regardless of the depth and extent of alteration. The $\delta^{30}Si$ values of the altered oceanic crust are in general agreement with the previous estimate of the global fresh MORBs ($-0.27 \pm 0.06‰$, 2SD; Savage et al., 2014), suggesting that either low-temperature seawater alteration or high-temperature hydrothermal alteration does not cause resolvable Si isotopic fractionation at the bulk-rock scale in the altered oceanic crust.

Because the altered oceanic crust could be partially melted during subduction or in the convective mantle, we estimated the Si isotope fractionation between the melt and residue minerals of the altered oceanic crust. Our calculations show that Si isotopes can be fractionated between the melt and residues enriched in garnet and clinopyroxene. Although the bulk altered oceanic crust has a mantle-like Si isotopic signature, the residual solids of the recycled altered oceanic crust could be enriched in light Si isotopes and the melt could be enriched in heavy Si isotopes. This indicates that melting and recycling of the subducted oceanic crust can produce heterogeneous Si isotope compositions in the convective mantle, which could contribute to the source of ocean island basalts with low $\delta^{30}Si$.

1. Introduction

Subduction is a critical process for chemical evolution and mass transfer on the Earth. As subducted sediments, oceanic/continental crust, and lithospheric mantle have distinct trace element and isotopic compositions compared with the depleted mantle, the contributions of the subducted slab to the mantle could be discerned via heterogeneities in the elemental concentrations and the radiogenic and stable isotopic compositions (e.g., Zindler and Hart, 1986; Hofmann, 1997; Hassler and Shimizu, 1998; Eiler, 2001; Deines, 2002; Elliott et al., 2006; Pringle et al., 2016). Based on the trace element ratios, radiogenic isotope variations (e.g., Sr, Nd, Pb, Hf, Os), and noble gas systematics (e.g., He and Ne), a number of mantle endmembers were defined, including DMM (depleted MORB mantle), HIMU (high μ, μ is the time-integrated $^{238}U/^{204}Pb$), EM1 (high $^{87}Sr/^{86}Sr$ and low $^{206}Pb/^{204}Pb$), EM2 (high $^{87}Sr/^{86}Sr$ and intermediate $^{206}Pb/^{204}Pb$), and FOZO (intermediate $^{87}Sr/^{86}Sr$, $^{143}Nd/^{144}Nd$, $^{206}Pb/^{204}Pb$, and high $^{3}He/^{4}He$) (e.g., Zindler and Hart, 1986; Hart and Hauri, 1992; Stracke et al., 2005). It has been accepted that involvement of recycled crustal materials is one of the key factors in producing the isotopic variations in the mantle (e.g., Chase, 1981; White and Hofmann, 1982; Zindler and Hart, 1986; Hauri and Hart, 1993; Hofmann, 1997; Graham, 2002; Jackson and Dasgupta, 2008; Day et al., 2009). Therefore, understanding the chemical and isotopic variability of subducted crustal material is crucial for the understanding of element cycling and its impact on the composition of the Earth's mantle.

Elements released from the altered oceanic crust could dramatically change the geochemical properties of the mantle wedge down to the lower mantle (e.g., Zindler and Hart, 1986; Hofmann, 1997; Hassler and Shimizu, 1998; Eiler, 2001; Deines, 2002; Elliott et al., 2006). Previous studies have shown that the complex hydrothermal processes result in resolvable isotopic fractionation of C, O, S, Li, Fe, Cu, and Zn in the altered oceanic crust (e.g., Hart et al., 1999; Furnes et al., 2001; Chan et al., 2002; Rouxel et al., 2003; Alt et al., 2010; Gao et al., 2012;

* Corresponding authors.
E-mail addresses: huy16@ustc.edu.cn (H.-M. Yu), fhuang@ustc.edu.cn (F. Huang).

https://doi.org/10.1016/j.chemgeo.2017.12.013
Received 1 April 2017; Received in revised form 1 December 2017; Accepted 19 December 2017
Available online 21 December 2017
0009-2541/

Huang et al., 2016), but some stable isotopes, such as Mg and V isotopes, may not be significantly affected during these processes (Prytulak et al., 2013; Huang et al., 2015).

Although Si is the third most abundant element of the bulk Earth (~16.1 wt%, McDonough, 2003), there are very few studies of Si isotope behavior during alteration of oceanic crust by seawater and hydrothermal fluids. Silicon isotopes have the potential to be a useful tool to constrain the recycling of the crust and evolution of the mantle (e.g., Savage et al., 2010, 2014; Pringle et al., 2016). Silicon isotopes can be significantly fractionated under a low-temperature environment by up to several per-mil during chemical weathering, mineral dissolution and precipitation, and biological activities (e.g., Basile-Doelsch et al., 2005; Ding et al., 2005; Ziegler et al., 2005; Delstanche et al., 2009; Opfergelt et al., 2009, 2010; Bern et al., 2010; Frings et al., 2016; Zheng et al., 2016). In these processes, the dissolved Si is generally enriched in ^{30}Si, and the precipitated phases (including secondary minerals and the biogenic silica) are ^{30}Si-depleted on average (Basile-Doelsch, 2006). Therefore, the dissolved Si in different water bodies, including groundwater, river, lake, seawater, and hydrothermal fluids generally have heavier average δ^{30}Si than the bulk silicate Earth (BSE) (-0.29 ± 0.06‰, Savage et al., 2014). For example, the average δ^{30}Si of river water is +1.1‰ (Basile-Doelsch et al., 2005), and seawater ranges between +0.6‰ and +3.1‰ (De La Rocha et al., 2000; Varela et al., 2004; Cardinal et al., 2005). In contrast, the bulk soils, secondary minerals, and siliceous precipitates have a lighter average δ^{30}Si than the BSE (e.g., Basile-Doelsch, 2006; Frings et al., 2016). The quartzs of silcretes have the lightest δ^{30}Si, ranging from −5.7‰ to −1.6‰ (Basile-Doelsch et al., 2005).

In contrast to the large Si isotopic variation observed from a low-temperature environment, igneous rocks and minerals only show limited Si isotopic variation (Georg et al., 2007; Fitoussi et al., 2009; Chakrabarti and Jacobsen, 2010; Savage et al., 2010, 2011, 2013a, 2013b, 2014; Armytage et al., 2011; Zambardi et al., 2013; Poitrasson and Zambardi, 2015). The main reservoirs of the Earth have similar average Si isotopic compositions. The δ^{30}Si of the Earth's mantle is -0.29 ± 0.08‰ (2SD; Savage et al., 2010, 2011), and of the oceanic crust is -0.32 ± 0.09‰ (2SD, Pringle et al., 2016). The δ^{30}Si of the lower, middle, and upper continental crust are -0.29 ± 0.04‰, -0.23 ± 0.04‰, and -0.25 ± 0.16‰, respectively (2SD, Savage et al., 2013a, 2013b), and are not significantly different from the mantle value. The similar δ^{30}Si values of igneous rocks are consistent with the result of first-principles calculations, which predict that the Si isotopes fractionation during magmatic differentiation is small (< 0.2‰, Huang et al., 2014; Wu et al., 2015; Qin et al., 2016).

As the top layer of subducted slab, the knowledge of Si isotopes of the altered oceanic crust is important for understanding how the subduction process could affect the Si isotope compositions of the mantle. To investigate the vertical variation in Si isotopic compositions of an intact oceanic crust and fractionation of Si isotopes during fluid alteration, we present the first Si isotope analyses on the altered oceanic crust samples recovered from IODP Site 1256 at the East Pacific Rise (EPR). From top to bottom, these samples have experienced low-temperature seawater alteration to high-temperature hydrothermal fluid alteration. Our results show that the bulk altered oceanic crust at IODP Site 1256 has a mantle-like Si isotopic composition with an average of δ^{30}Si = -0.32 ± 0.06‰ (2SD, $N = 50$). We further estimate Si isotopic composition of melts and solid residue of the melted oceanic crust to constrain the possible impacts on mantle heterogeneities.

2. Sample location and description

IODP Site 1256 (6°44.2′N, 91°56.1′W) is located in the Guatemala Basin on the Cocos Plate, the eastern side of the EPR. IODP Site 1256 has two drilling holes, 1256C and 1256D. Hole 1256C cored the uppermost lavas, including a 250.7 m sediment section, and an 88.5 m basement section (Fig. 1; Wilson et al., 2003). Hole 1256D is ~30 m south of 1256C and starts at 276 m below seafloor (mbsf) without sediment section. This hole penetrates through the (1) volcanic section, (2) transition zones, (3) sheeted dyke complex, and (4) plutonic section (Fig. 1; Wilson et al., 2003, 2006; Teagle et al., 2006, 2012).

Based on O and Li isotope data, the core samples of IODP Site 1256 show significant alteration with highly variable temperatures and water/rock (w/r) ratios (Gao et al., 2012). The volcanic section includes a lava pond (~276–350.3 mbsf), inflated flows (350.3–533.9 mbsf), and sheet and massive flows (533.9–1004.2 mbsf). The whole volcanic section is slightly or moderately altered, with a highly altered interval (41 cm) occurring at 648 mbsf, which might be a narrow zone of focused fluid flow (Alt et al., 2010). The upper part of the volcanic zone (~276–964 mbsf) was altered by low-temperature seawater under reducing conditions (< 100 °C), and the lower part of the volcanic zone (964–1004.2 mbsf) was altered under elevated temperatures (100–200 °C; Teagle et al., 2006; Alt et al., 2010). The transition zone (1004.2–1060.9 mbsf) is characterized by subvertical intrusive contacts with more intense alteration than in the overlying volcanic section (Teagle et al., 2006). This section is a mixing zone between upwelling hydrothermal fluid alteration and down-welling seawater alteration, and the change from the two alterations occurs over a narrow interval in this zone (Alt et al., 2010). The upper extrusive basalts above the transition zone (1004.2–1060.9 mbsf) of IODP Site 1256 mainly experienced low-temperature (< 200–250 °C) seawater alteration. The sheeted dyke complex and plutonic section below the transition zone experienced high-temperature alteration (> 250–500 °C) from upwelling hot hydrothermal fluids (Alt et al., 2010; Gao et al., 2012). The sheeted dyke complex (1060.9–1406.6 mbsf) was highly altered from top to bottom, with alteration temperatures increasing downward from 250 to 400 °C (Teagle et al., 2006; Alt et al., 2010). The lower sheeted dykes (1348.3–1406.6 mbsf) display distinctive granoblastic textures formed by partial to complete recrystallization due to contact metamorphism at or near magmatic temperatures with underlying gabbroic intrusions (Koepke et al., 2008; France et al., 2009; Alt et al., 2010). The plutonic complex (1406.6–1507.1 mbsf) has similar metamorphic conditions as the lower dykes (Alt et al., 2010). It contains two gabbro bodies separated by a granoblastically recrystallized dyke, and the margins of the two gabbro bodies are moderately altered with secondary minerals (Teagle et al., 2006).

The δ^{7}Li value of the bulk rock reaches a minimum at ~1350 mbsf, which reflects a low w/r ratio (w/r < 1; Fig. 1; Gao et al., 2012). Above the transition zone, most of the samples experienced high w/r ratio alteration, except the sample around 536 mbsf. Below the transition zone, the w/r ratios of alterations decrease with increasing depth (Gao et al., 2012). In addition, the samples from IODP Site 1256 have been extensively studied for major and trace element contents as well as Mg, Fe, Cu, and Zn isotopic compositions (Wilson et al., 2003, 2006; Teagle et al., 2006; Neo et al., 2009; Gao et al., 2009, 2012; Dziony et al., 2014; Huang et al., 2015, 2016). This study presents Si isotopic data of one basalt from Hole 1256C and 45 samples (including 36 basalts, 1 dolerite, 3 gabbronorites, and 5 gabbros) from Hole 1256D.

3. Analytical methods

3.1. Sample digestion and chemical purification procedures

Chemical purification procedures were performed in an ISO-class 6 clean room in the CAS Key Laboratory of Crust-Mantle and Environments at the University of Science and Technology of China (USTC), Hefei. The concentrated acids used in this study were high purity after double distillation. All reagents were then diluted from the concentrated acids with ultra-pure water (18.2 MΩ·cm).

The purification procedure is modified from the method of Georg et al. (2006). Briefly, sample powders were digested by the alkali fusion method (Potts, 1987). The sample powder (4.5–5 mg) was well mixed

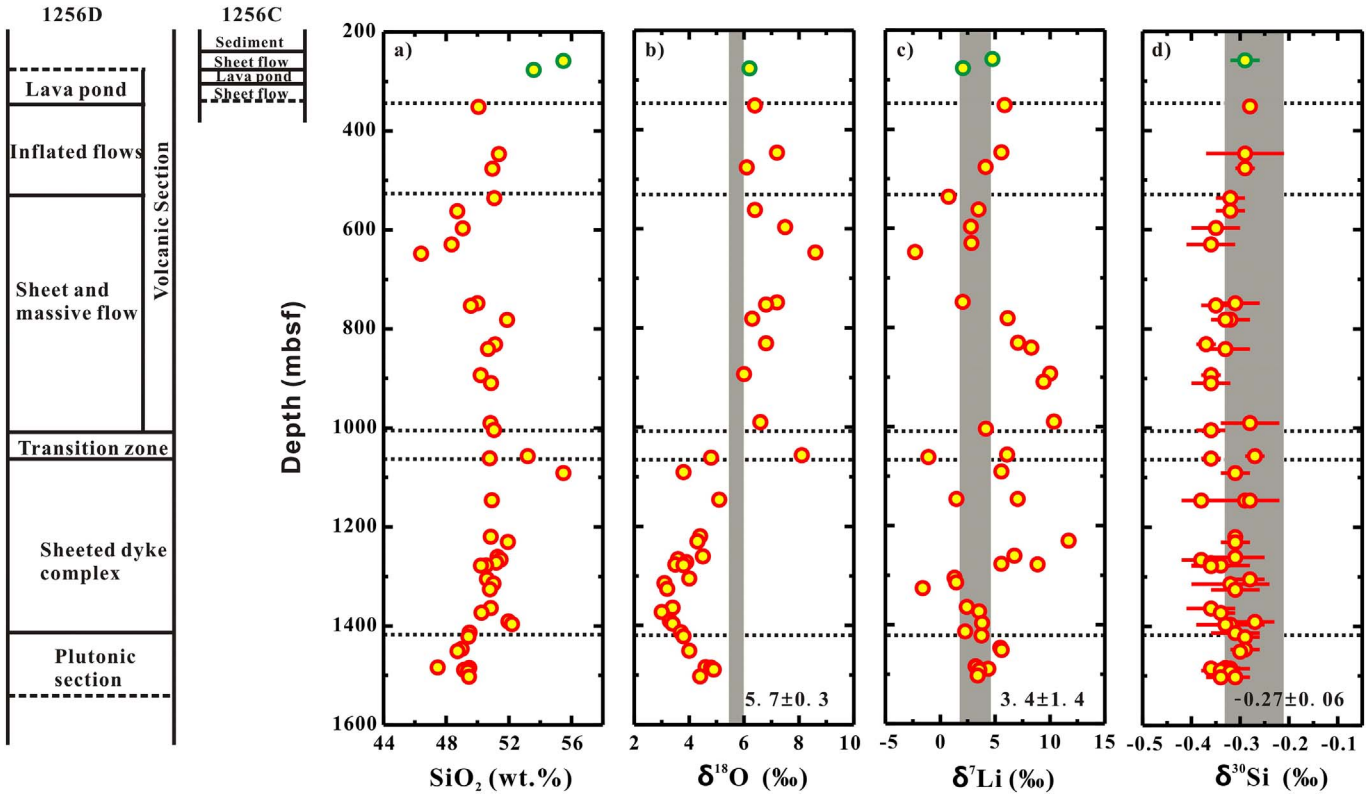

Fig. 1. The profile of the altered oceanic crust from the IODP Site 1256C and 1256D (modified from Gao et al., 2012), with the down hole variation in SiO_2 content, O, Li, and Si isotope compositions. The (a) SiO_2 content of IODP Site 1256 core samples are from Neo et al. (2009), Teagle et al. (2006), Wilson et al. (2003, 2006); (b) $\delta^{18}O$; and (c) $\delta^{7}Li$ values are from Gao et al. (2012). The gray bars are the average isotopic compositions of $\delta^{18}O$, $\delta^{7}Li$, and $\delta^{30}Si$ in the fresh MORBs (Harmon and Hoefs, 1995; Tomascak et al., 2008; Savage et al., 2014). The green circles denote samples from 1256C and red circles denote samples from 1256D. (For interpretation of the references to color in this figure legend, the reader is referred to the web version of this article.)

with alkali flux (~120 mg of high purity NaOH powder), and heated in a silver crucible (with lid) at 720 °C for 10 min to produce a water-soluble metastable silicate. When the crucible cooled, the outside and the bottom of the crucible were carefully cleaned with water to get rid of any possible contamination, and then the crucible was placed into a 60 mL Teflon vial with ~20 mL water and allowed to sit on a hotplate over 12 h at 80 °C. After the crucible was removed from the Teflon vial, enough HNO_3 was added to the sample solution in the Teflon vial to attain a solution acidity of 1% HNO_3 (v/v) for column chemistry.

The sample solution (containing ~30 μg Si) was purified through 2 mL of cation exchange resin (AG50W-X12, 200–400 mesh, Bio-Rad, USA). The resin was first cleaned with 3 mol/L HNO_3, 6 mol/L HNO_3, and 6 mol/L HCl alternatively (three bed volumes for each reagent), after which the resin was conditioned with water (6 mL) before loading the sample. The sample was then loaded onto the column in 1 mL of 1% HNO_3. Silicon was collected right after the sample solution was loaded, and it was further eluted with 6 mL of water. Next, 1 mL water was added to the column and collected to test whether the Si elution curve drifted during the chromatographic process. The yields of all our samples were > 99%. The total procedural blank was ~20 ng, which is negligible relative to the ~30 μg Si loaded into the column.

3.2. Mass spectrometry analyses

Silicon isotope ratios were analyzed using the MC–ICP–MS (Neptune Plus from Thermo-Fisher Scientific) in the CAS Key Laboratory of Crust-Mantle and Environments at the USTC. Nickel cones (H skimmer and Jet sampler cones; Thermo-Fisher Scientific), a quartz dual cyclonic spray chamber (ESI), and a PFA microflow nebulizer (ESI) with an uptake rate of ~50 μL/min were used for sample introduction. The three stable isotopes of Si, ^{28}Si (92.23%), ^{29}Si (4.68%), and ^{30}Si (3.09%), were collected by Faraday cups L3, C, and H3, respectively. At medium resolution (resolution > 5500), the peaks of ^{28}Si, ^{29}Si, and ^{30}Si were partially resolved from molecular interferences (such as $^{28}SiH^+$, $^{12}C^{16}O^+$, $^{14}N_2^+$, and $^{14}N^{16}O^+$) with a flat-topped shoulder on the lower mass side of the mixed peaks. The sensitivity of ^{28}Si was ~5 V/ppm at medium resolution. The mass bias of the instrument during isotope measurements was corrected using the sample-standard bracketing method (SSB), and the Si isotope data were reported in the standard δ-notation in per mil relative to the standard reference material NBS-28 $\left(\delta^{30}Si = \left(\frac{\left(\frac{^{30}Si}{^{28}Si}\right)_{sample}}{\left(\frac{^{30}Si}{^{28}Si}\right)_{NBS-28}} - 1\right) \times 1000\right)$. Each sample was bracketed before and after by standard NBS-28, with usually three or four repeated analyses of the same sample solution.

The precision and accuracy of Si isotope analyses were determined via measurements of the Si isotopes of rock standards from the United States Geological Survey (USGS) (e.g., BHVO-2, BCR-2, AGV-1, and AGV-2), and replicated samples. The results of the measurements of USGS standards are consistent with values reported in the literature within error (Table 1). All replicated samples are consistent with each other within error (Table 1). The $\delta^{30}Si$ of BHVO-2 has been measured in our lab in the last two years and the measured value is -0.29 ± 0.05‰ ($n = 159$, 2SD; Fig. 2; Table 1A). In a three-isotope plot (Fig. 3), all samples and rock standards (BHVO-2, BCR-2, AGV-1, and AGV-2) analyzed in this study are consistent with the calculated equilibrium ($\delta^{29}Si = 0.5178 \times \delta^{30}Si$) or kinetic ($\delta^{29}Si = 0.5092 \times \delta^{30}Si$) fractionation lines within error, following the mass-dependent fractionation law (Young et al., 2002).

Table 1
Silicon isotopic compositions of international rock standards from USGS reported in this study and in the literature.

		δ^{29}Si (‰)	2SD (2SE)	δ^{30}Si (‰)	2SD (2SE)	*n*
BHVO-2	This study	− 0.15	0.03	− 0.30	0.05	24
	Abraham et al. (2008)[a]	− 0.17	0.04	− 0.29	0.11	
	Fitoussi et al. (2009)[a]	− 0.16	0.04	− 0.32	0.04	14
	Savage et al. (2010)	− 0.14	0.05	− 0.27	0.10	192
	Armytage et al. (2011)[b]	− 0.16	0.02	− 0.31	0.04	4
	Zambardi and Poitrasson (2011)[a]	− 0.14	0.05	− 0.27	0.08	42
BCR-1	Savage et al. (2010)	− 0.13	0.03	− 0.28	0.07	14
	Zambardi and Poitrasson (2011)[a]	− 0.11	0.05	− 0.19	0.07	6
BCR-2	This study	− 0.06	0.05	− 0.21	0.06	6
AGV-1	This study	− 0.09	0.01	− 0.18	0.04	3
AGV-2	This study	− 0.09	0.06	− 0.21	0.00	3
	Savage et al. (2011)	− 0.10	0.03	− 0.21	0.07	11
	Zambardi and Poitrasson (2011)[a]	− 0.07	0.05	− 0.15	0.06	6

[a] Uncertainties are expressed as ± 2SE (standard error). All data from this study and other literature are expressed as ± 2SD (standard deviation).
[b] The data are from the average of BHVO-1 and -2 in Armytage et al. (2011).

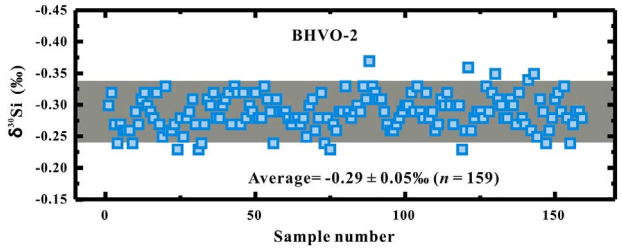

Fig. 2. The δ^{30}Si values of the international rock standard of BHVO-2 analyzed in two years. The long-term external precision of δ^{30}Si is ± 0.05‰ (2SD) in the CAS Key Laboratory of Crust-Mantle and Environments at the USTC.

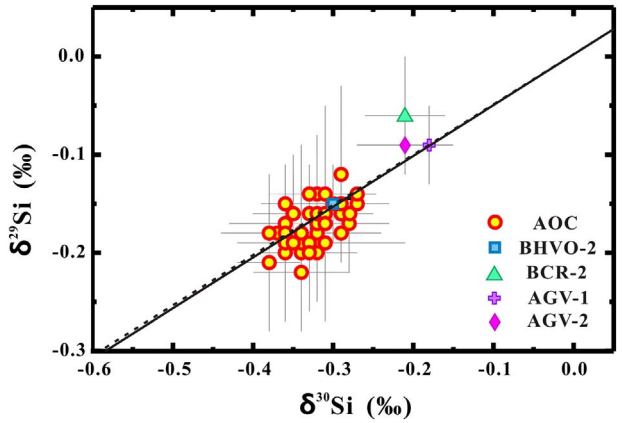

Fig. 3. Three-isotope plot of δ^{30}Si vs. δ^{29}Si in this study. All core samples of IODP Site 1256 and four international rock standards are on the calculated mass-dependent equilibrium (solid line) and kinetic (dashed line) fractionation lines within error (± 2SD) (Young et al., 2002).

4. Results

The Si isotopic compositions of the core samples of IODP Site 1256 are reported in Table 2. The sample information, the SiO_2 (wt%) content, chemical index of alteration (CIA, defined in molar ratio as $Al_2O_3/(Al_2O_3 + CaO^* + Na_2O + K_2O) \times 100$, where CaO* is the CaO that is not from carbonate or phosphate; Nesbitt and Young, 1982) and loss on ignition (LOI) data of these samples are from Gao et al. (2012). Although the SiO_2 content of the samples varies between 47.45 and 55.48% (wt%), the variation in Si isotopic composition is very small (Fig. 1 and Table 2). The δ^{30}Si values of our samples range from − 0.38 to − 0.27‰, with an average value of − 0.32 ± 0.06‰ (2SD, $N = 50$). This average value is identical to that of global fresh MORBs (− 0.27 ± 0.06‰) and the BSE (− 0.29 ± 0.07‰) (Savage et al., 2014). The δ^{30}Si of the altered oceanic crust samples do not show any correlation with sampling depth and extent of alteration.

5. Discussion

5.1. Limited Si isotopic fractionation during oceanic crust alteration

The Si isotopes could be fractionated during weathering due to the dissolution of primary minerals or secondary minerals precipitation (e.g., Ziegler et al., 2005; Chemtob et al., 2015; Prentice and Webb, 2016). Some preliminary experimental studies have shown that ^{30}Si will preferentially move into solution relative to ^{28}Si during mineral dissolution from weathering (Ziegler et al., 2005; Chemtob et al., 2015; Prentice and Webb, 2016). It is also possible that when basalt was dissolved in dilute hydrofluoric acid in the environment during weathering, the isotopically light Si was preferentially released to produce secondary minerals with high δ^{30}Si (Chemtob et al., 2015). Based on the CIA and LOI of these altered oceanic crust samples, most samples did not experience strong weathering (Fig. 4a and b). The δ^{30}Si of these samples did not correlate with either CIA or LOI (Fig. 4a and b), supporting the view that the weathering process in the altered oceanic crust of IODP Site 1256 did not significantly change the Si isotope compositions. There is no correlation between δ^{30}Si and Mg# either (Fig. 4c), indicating that the Si isotope compositions of these samples were not affected by magma differentiation in the oceanic crust.

Most altered oceanic samples have homogeneous Si isotope compositions similar to fresh MORBs regardless of the depths or rock types (Fig. 1). The variable δ^{18}O and δ^{7}Li values of these samples reflect different alteration temperatures and w/r ratios, respectively (Gao et al., 2012). No correlation between δ^{30}Si and δ^{18}O or δ^{7}Li is observed, indicating that both seawater alteration and hydrothermal alteration did not fractionate Si isotopes in the altered oceanic crust at the bulk-rock scale, despite the highly variable alteration temperatures and w/r ratios. This could be attributed to the much higher Si concentration of the oceanic crust relative to those of seawater and hydrothermal fluids. The highest observed D_{Si} (dissolved Si) in the global ocean is ~170 μmol/L (or 0.00048 wt%). The hydrothermal fluids might have higher D_{Si} concentrations of up to 11–15 mmol/L (or 0.031–0.042 wt%) based on two samples reported in a previous study (De La Rocha et al., 2000). Compared with the high SiO_2 contents in oceanic crust (> 47 wt % in this study), the D_{Si} in seawater and hydrothermal fluids are almost negligible. Therefore, even though seawater has a large variation in δ^{30}Si from ~0.5 to 3‰ (van den Boorn et al., 2007; Frings et al., 2016), which is much heavier than the average of igneous rocks, the alteration process still did not affect Si isotopes in the altered oceanic crust.

A previous study observed the clay minerals and veins existing in the core samples of Drilling Hole 1256 (Alt et al., 2010). Although the

Table 2
Silicon isotopic compositions of the IODP Site 1256 core samples relative to NBS-28 as bracketing standard.

Sample	T-B (cm)	Depth (mbsf)	Sample description	SiO_2 (wt%)	LOI	CIA	$\delta^{29}Si$ (‰)	2SD	$\delta^{30}Si$ (‰)	2SD	*n*
6R/2	3–11	258.46	Coarse-grained altered basalt	55.48	NA	41.1	− 0.16	0.02	− 0.29	0.03	3
12R/8	71–79	351.21	Microcrystalline basalt	50.06	2.30	36.5	− 0.16	0.08	− 0.28	0.01	3
27R/1	130–137	446.7	Microcrystalline basalt	51.36	0.30	36.6	− 0.16	0.07	− 0.29	0.08	3
32R/1	114–120	476.34	Microcrystalline basalt	50.94	0.20	36.8	− 0.12	0.02	− 0.29	0.02	3
43R2W	48–54	535.88	Patchy altered basalt	51.07	0.80	36.7	− 0.17	0.03	− 0.32	0.03	3
46R1W	67–69	562.17	Altered basalt	48.71	3.90	41.3	− 0.17	0.08	− 0.32	0.03	3
51R1	52–54	596.62	Altered basalt	49.06	7.00	41.3	− 0.19	0.07	− 0.35	0.05	3
55R2W	64–68	629.48	Microcrystalline basalt	48.34	0.20	36.6	− 0.18	0.09	− 0.36	0.05	3
74R1W	118–122	748.38	Patchy basalt	50.00	0.58	36.3	− 0.16	0.11	− 0.31	0.05	3
75R/1	131–133	753.05	Patchy basalt	49.58	1.69	37.3	− 0.16	0.04	− 0.35	0.03	3
80R/1	103–107	781.47	Aphyric cryptocrystalline basalt	51.88	1.27	37.8	− 0.20	0.02	− 0.32	0.04	3
80R/2	92–102	781.47	Fine-grained basalt with mixed halo	51.88	1.27	37.8	− 0.20	0.02	− 0.33	0.02	3
87R/2	66–68	831.06	Phyric fine-grained basalt	51.12	0.63	35.7	− 0.18	0.04	− 0.37	0.02	3
89R/1	70–73	840.68	Phyric cryptocrystalline basalt	50.67	0.66	36.4	− 0.14	0.00	− 0.33	0.05	3
96R/1	29–31	893.29	Aphyric microcrystalline basalt	50.20	NA	36.1	− 0.18	0.05	− 0.36	0.02	3
99R/2	101–120	909.63	Fine-grained basalt	50.86	0.46	36.1	− 0.15	0.03	− 0.36	0.04	3
114R/2	54–56	990.04	Altered phyric microcrystalline basalt	50.83	0.96	37.1	− 0.16	0.05	− 0.28	0.06	3
117R/1	97–107	1004.17	Fine-grained cataclastic basalt	51.05	2.45	38.9	− 0.17	0.04	− 0.36	0.03	3
128R/1	58–63	1056.77	Fine-grained basalt	53.21	1.38	35.2	− 0.14	0.03	− 0.27	0.02	3
129R/1	34–51	1061.51	Fine-grained basalt	50.78	1.01	35.4	− 0.18	0.07	− 0.36	0.02	3
135R/1	54–64	1090.86	Patchy microcrystalline basalt	55.49	4.71	42.5	− 0.14	0.01	− 0.31	0.03	3
147R/1	40–48	1145.98	Doleritic basalt	50.92	2.13	36.1	− 0.15	0.03	− 0.29	0.07	3
147R/1-R							− 0.17	0.10	− 0.28	0.06	3
147R/1	75–77	1145.98	Aphyric fine-grained dolerite	50.92	2.13	36.1	− 0.21	0.07	− 0.38	0.04	3
163R/3	59–62	1219.91	Phyric cryptocrystalline basalt	50.84	1.86	36.4	− 0.16	0.08	− 0.31	0.01	3
165R/3	101–103	1230.19	Aphyric microcrystalline basalt	51.94	1.64	35.4	− 0.19	0.08	− 0.31	0.03	3
173R/2	6–10	1260.6	Phyric medium-to fine-grained basalt	51.27	1.09	36.2	− 0.17	0.02	− 0.31	0.06	3
174R/1	130–134	1266.13	Aphyric fine-grained basalt	51.47	1.33	37.2	− 0.18	0.06	− 0.38	0.04	3
175R/1	58–62	1272.05	Aphyric cryptocrystalline basalt	51.19	1.04	36.3	− 0.19	0.05	− 0.36	0.01	3
176R/1	133–136	1277.27	Aphyric fine-grained basalt	50.54	1.42	36.5	− 0.22	0.06	− 0.34	0.06	3
176R/2	22–25	1278.03	Aphyric fine-grained basalt	50.22	1.00	37.1	− 0.20	0.07	− 0.36	0.04	3
182R/1	25–28	1305.09	Aphyric fine-grained basalt	50.60	0.28	36.4	− 0.16	0.09	− 0.28	0.03	3
184R/1	98–104	1314.5	Aphyric fine-grained basalt	51.02	0.45	36.2	− 0.16	0.06	− 0.32	0.08	3
187R/1	15–17	1325.88	Aphyric microcrystalline basalt	50.79	0.39	36.5	− 0.19	0.00	− 0.31	0.05	3
196R/1	30–32	1363.86	Aphyric fine-grained basalt	50.84	0.22	36.1	− 0.18	0.01	− 0.36	0.05	3
202R/1	37–42	1373.05	Aphyric fine-gained basalt	50.25	0.00	37.3	− 0.20	0.02	− 0.34	0.03	3
207R/1	10–15	1390.8	Aphyric cryptocrystalline basalt	51.97	NA	36.2	− 0.15	0.01	− 0.27	0.04	3
209R/1	15–19	1396.65	Aphyric microcrystalline basalt	52.20	NA	36.1	− 0.18	0.06	− 0.32	0.07	3
209R/1-R							− 0.19	0.07	− 0.33	0.06	3
214R/2	50–55	1413.55	Disseminated oxide gabbro	49.49	0.46	36.0	− 0.17	0.07	− 0.31	0.05	3
217R/1	4–9	1421.77	Disseminated oxide gabbro	49.42	0.71	35.3	− 0.18	0.04	− 0.29	0.03	3
222R/2	25–35	1446.37	Green altered gabbro	48.99	0.61	35.4	− 0.16	0.03	− 0.29	0.03	3
223R/2	41–48	1450.68	Olivine gabbronorite	48.72	1.66	35.7	− 0.15	0.01	− 0.30	0.01	3
230R/1	68–72	1483.72	Fine-grained opx bearing oxide gabbro	47.45	0.15	35.1	− 0.16	0.03	− 0.33	0.03	3
230R/2	36–40	1484.99	Disseminated oxide gabbro-gabbronorite	49.47	0.68	35.0	− 0.20	0.06	− 0.36	0.01	3
230R/2-R							− 0.14	0.05	− 0.32	0.04	3
231R/3	21–27	1488.8	Oxide gabbronorite	49.14	0.86	34.4	− 0.18	0.01	− 0.34	0.04	3
231R/3	80–98	1491.36	Opx bearing gabbro	49.39	0.51	34.4	− 0.14	0.03	− 0.32	0.02	3
234R/1	19–22	1502.76	Fine-grained basalt	49.46	2.19	34.2	− 0.17	0.07	− 0.31	0.03	3
234R/1-R							− 0.19	0.06	− 0.34	0.03	3

147R/1-R, 209R/1-R, 230R/2-R, and 234R/1-R are the replicated samples of 147R/1, 209R/1, 230R/2, and 234R/1, respectively.
The sample information, including sample names, thickness, depths, descriptions and SiO_2 contents, are from Gao et al. (2012).

clay minerals or veins in the drilling hole could have large Si isotopic variations (e.g., Ziegler et al., 2005; Chemtob et al., 2015; Prentice and Webb, 2016), the bulk core samples have homogeneous $\delta^{30}Si$. This indicates that clay minerals or veins in the core samples did not affect the $\delta^{30}Si$ of altered oceanic crust on the bulk-rock scale. This is either because the amount of the clay minerals or veins is limited (< 1%) (Alt et al., 2010), or the alteration degree is too low to produce obvious Si isotope fractionation.

5.2. Silicon isotopic fractionation in the recycled crustal materials

Dehydration and partial melting processes could happen in the subducted altered oceanic crust. It is unclear whether the subducted slab could produce or preserve heterogeneous Si isotope signatures in the mantle after dehydration and/or partial melting. Arc basalts may provide some useful information because they could reflect the signature of fluids or melts from a subducted slab. The $\delta^{30}Si$ data of arc basalts are still rare. There are only three samples from the Marianas arc and one sample from the South Sandwich arc that have been analyzed for Si isotopes. Although the mantle source of these arc basalts was metasomatized by recycled sediments or fluids, the basalts all exhibit MORB-like Si isotopic compositions ($\delta^{30}Si_{arc\ basalts} = -0.28 \pm 0.06$‰; Savage et al., 2010), indicating that either the fluids from the subducted slab have $\delta_{30}Si$ similar to the mantle, or that the Si content of the released fluids is too low to impact Si isotopic composition of the mantle wedge. Therefore, metamorphic dehydration may not strongly affect the Si isotope composition of the dehydrated slab.

It is also important to understand whether the partial melting process could fractionate Si isotopes in the subducted slab. To estimate this effect, we calculate the Si isotopic fractionation between residue minerals and melts after melting, based on their reduced partition function ratios of $^{30}Si/^{28}Si$ ($10^3 ln\beta$). The $10^3 ln\beta$ of melts and different minerals can be obtained from first-principles calculations (Huang et al., 2014; Wu et al., 2015; Qin et al., 2016). Experimental studies for partial

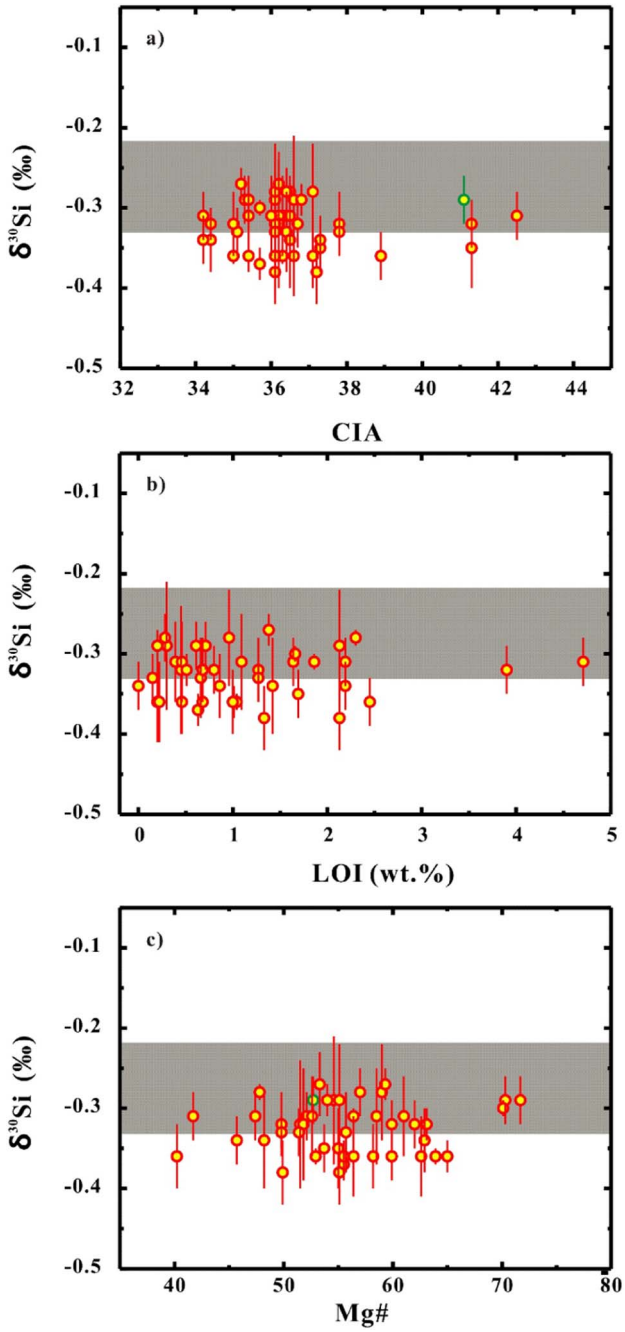

Fig. 4. Plots of δ^{30}Si versus (a) CIA, (b) LOI, and (c) Mg# of the altered oceanic crust samples from the IODP Site 1256. The parallel gray bars represent the average δ^{30}Si value of fresh MORBs (Savage et al., 2014).

melting of high-temperature and pressure eclogites (i.e., subducted oceanic crust) show that melts from mafic lithologies are highly variable in composition at different melting fractions. Therefore, we choose the proportion and compositions of melts and residue minerals of melted eclogites from the experimental data with different temperature and pressure conditions (Spandler et al., 2008). The starting material of the experiment is an anhydrous alkali-rich basalt (GA2) whose composition was used to represent the sea-floor-altered mid-ocean ridge basalt after dehydration (Spandler et al., 2008). The melting pressure and temperature conditions are from 3.0 to 5.0 GPa and from 1200 to 1600 °C, respectively. To simplify the calculation, we only choose the experimental results with garnet and clinopyroxene (cpx) as the dominant residual silicate minerals because they are the main minerals of eclogites. The 10^3lnβ of melts were calculated using the model of Table S2 of Qin et al. (2016), and the 10^3lnβ of minerals in the residue (garnet and cpx) were calculated using the parameters in Table 1 of Huang et al. (2014). The δ^{30}Si of BSE (−0.29‰) is selected as the original Si isotope composition of the bulk oceanic crust (Savage et al., 2014). All the calculation results are listed in Table 3.

These results show that all melts have heavier δ^{30}Si than residue minerals (garnet and cpx; Table 3 and Fig. 5). When the melting degree is low (< 20%), the δ^{30}Si of the melt could be much higher than the average ratio of the upper mantle, but the δ^{30}Si of residue minerals are close to the MORB values (Fig. 5). With the melting degree increasing, the melt fraction increases and the δ^{30}Si of the melt decreases toward the average of the MORB values. In contrast, the δ^{30}Si of the residue minerals decreases and becomes lower than the MORB values (Fig. 5). The heaviest δ^{30}Si in the melt is −0.07 ± 0.05‰ when the starting material is melted at 1280 °C under 3 GPa with 21% of melt. A previous study suggested that the eclogites could stop melting at melt fractions of > 50% (under near fractional melting conditions) because the residue is too refractory (Sobolev et al., 2005). Nonetheless, we calculate the Si isotope compositions with melt fractions higher than 50% (using the compositions of batch melting) for the purpose of illustration. In this study, we mainly discuss Si isotope compositions of residue minerals produced with partial melting degree lower than 50% (Table 3). With temperature and the partial melting degree increasing, the δ^{30}Si of residue garnet and cpx get lighter. For example, the δ^{30}Si of garnet and cpx are −0.39‰ and −0.40‰, respectively, with melt fraction of 36% at 1360 °C and 3 GPa (Table 3). Compared with Si isotopes of MORBs (−0.27 ± 0.06‰, 2SD; Savage et al., 2014) and BSE (−0.29 ± 0.07‰, 2SD; Savage et al., 2014), these residue minerals have lighter Si isotope compositions.

The δ^{30}Si values of altered oceanic crust reported in Table 2 vary from −0.27‰ to −0.38‰. If δ^{30}Si of the bulk altered oceanic crust is set as −0.38‰ instead of the BSE value used in earlier modeling, the Si isotopes of residue minerals would be even lighter. The δ^{30}Si of residue garnet and cpx are −0.48‰ and −0.49‰, respectively, with melt fraction of 36% at 1360 °C and 3 GPa (Table 3).

Based on these results, we conclude that the melting of subducted slabs may result in substantial Si isotope heterogeneity in the mantle. It has been suggested that the fluid or the melt released from the subducted sediments could have a heterogeneous Si isotopic signature because of the large δ^{30}Si variation of sediments (Robert and Chaussidon, 2006; van den Boorn et al., 2007, 2010; Chakrabarti et al., 2012). Alternatively, even if the subducted crustal material has a homogeneous Si isotope composition (e.g., the altered oceanic crust of IODP Site 1256), the melt derived from the altered oceanic crust could be enriched with heavy Si isotopes and the residue solid could have light δ^{30}Si. The offset of δ^{30}Si between the melt and residue could be of 0.2–0.3‰, which is much larger than the current precision of Si isotope analyses (< 0.05‰, 2SD).

5.3. Tracing recycled crustal materials in the mantle using Si isotopes

Studies of ultramafic xenoliths, MORB, and island-arc basalts have revealed only limited Si isotopic variation in the Earth's mantle (Georg et al., 2007; Fitoussi et al., 2009; Chakrabarti and Jacobsen, 2010; Savage et al., 2010, 2011, 2013a, 2013b, 2014; Armytage et al., 2011; Zambardi et al., 2013; Poitrasson and Zambardi, 2015). However, a recent study showed lighter δ^{30}Si values (−0.46 to −0.28‰) in some HIMU-type ocean island basalt (OIB) samples from Mangaia, Cape Verde, and Iceland (Pringle et al., 2016), which indicates that there are components in the mantle with heterogeneous Si isotope compositions. It also supports that even though Si is a major element of the Earth's mantle, it is still possible that the Si isotope signatures of the subducted materials can be preserved in the mantle, and further observed in OIB.

One possible source of these HIMU-type OIB is the subducted oceanic sediment, which has highly heterogeneous δ^{30}Si (> 10‰) and is possibly enriched in light Si isotopes (Robert and Chaussidon, 2006;

Table 3
The parameters used to calculate the Si isotopes of melts and residue minerals in the subducted slab after partial melting, and the δ^{30}Si of different phases calculated based on first-principles calculation.

Sample		MH13	MH8	MH12	MH20	MH21	MH23	MH22	MH28	MH31	MH29
Melt (%)		21	36	61	85	23	53	86	21	46	68
Garnet (%)		35	27	22	14	32	24	14	33	28	17
Cpx (%)		44	37	17		45	23		46	26	15
P (Gpa)		3	3	3	3	4	4	4	5	5	5
T (°C)		1280	1360	1400	1440	1400	1450	1500	1400	1500	1550
Average major-element (wt% oxides) compositions of experimental melts	SiO_2	63.99	57.86	53.64	52	58.4	53.69	51.66	58.12	53.93	52.42
	TiO_2	2.77	2.94	2.25	2	4.13	2.9	1.95	4.37	3.17	2.35
	Al_2O_3	15.25	16.32	16.72	16.42	14.3	15.67	16.02	13.82	15.14	15.76
	FeO	4.66	7.54	9.08	9.1	7.81	9.79	9.69	8.16	9.9	9.62
	MgO	1.67	3.02	5.38	7.04	2.9	4.77	7.15	2.89	4.65	6.35
	CaO	4.34	6.54	8.32	9.19	6.53	8.41	9.38	6.92	8.39	9.17
	Na_2O	5.21	4.53	4.02	3.5	3.7	3.65	3.53	3.44	3.59	3.52
	K_2O	1.75	1.05	0.58	0.46	1.65	0.77	0.46	1.74	0.89	0.58
	P_2O_5	0.37	0.19		0.21	0.59	0.25	0.16	0.53	0.33	0.23
Garnet	SiO_2	–	39.69	–	–	40.21	40.47	41.85	40.15	40.92	40.69
Cpx	SiO_2	51.54	50.38	50.99	–	52.25	51.58	–	53.21	–	52.32
$1000\ln\beta_{30-28}$	Melt	3.301	2.968	2.801	2.669	2.836	2.646	2.492	2.834	2.502	2.357
	Garnet	3.012	2.718	2.587	2.465	2.603	2.451	2.312	2.620	2.326	2.198
	Cpx	3.004	2.711	2.580	2.459	2.601	2.449	2.310	2.622	2.329	2.201
δ^{30}Si	Melt	− 0.07	− 0.14	− 0.21	− 0.27	− 0.12	− 0.21	− 0.27	− 0.13	− 0.20	− 0.24
	Garnet	− 0.36	− 0.39	− 0.43	− 0.47	− 0.35	− 0.40	− 0.45	− 0.34	− 0.38	− 0.40
	Cpx	− 0.37	− 0.40	− 0.43		− 0.35	− 0.40		− 0.34	− 0.38	− 0.40

All data of proportions of different phases, temperature, pressure, and major element compositions are from the experimental data of Spandler et al. (2008). The SiO_2 (wt%) of garnet of MH13, MH12, and MH20, and cpx of MH31 were not reported in the literature. We estimated them as 39.5%, 40.0%, 40.0%, and 52.5%, respectively, based on the SiO_2 (wt%) of other garnet and cpx.

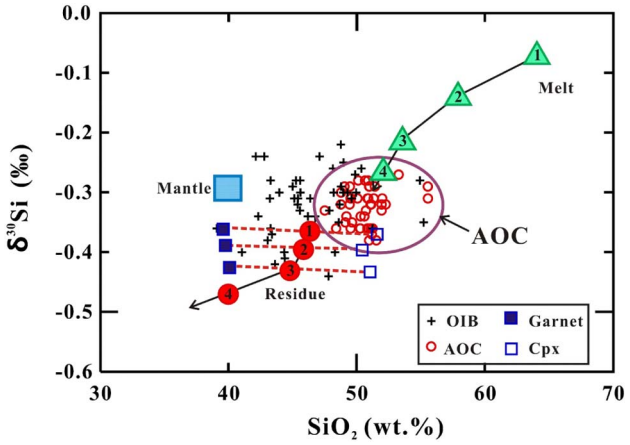

Fig. 5. The δ^{30}Si of OIB samples from Pringle et al. (2016), altered oceanic crust samples from this study, and the calculated δ^{30}Si in melts and residue minerals (garnet and cpx) under different temperatures. The numbers 1, 2, 3, and 4 in the triangle and circle symbols represent the melting degrees of 21%, 36%, 61%, and 85% under 3 GPa, respectively.

van den Boorn et al., 2007, 2010; Chakrabarti et al., 2012). However, the majority of sediments overlying the oceanic crust may be scraped off into the accretion zone during subduction before entering the convecting mantle (Clift and Vannucchi, 2004). The addition of a few percent of sediments in the mantle source could not produce the observed Pb and Sr isotopic signatures and trace element ratios in the HIMU-type basalts (Roy-Barman and Allègre, 1995; Chauvel et al., 2008). For these reasons, the recycled oceanic sediments are unlikely to be the source of OIB with light Si isotopic signatures.

Another possible source for these OIB with lower δ^{30}Si is the residue of recycled oceanic crust after partial melting. Although the results of our study show that bulk altered oceanic crust has only limited Si isotope variation, the residue minerals could have lower δ^{30}Si after partial melting (Table 3 and Fig. 5). Calculations from a previous study have shown that if the recycled component with δ^{30}Si of − 0.5‰ contributes 25% of the mass of lava, it could produce the light δ^{30}Si signatures observed from these HIMU and Iceland OIB (Pringle et al., 2016). Based on our calculations, the residue minerals could have δ^{30}Si of − 0.39 ± 0.05‰ or even lower with higher degree melting. If the subducted slab is hot, it could melt under a lower pressure to produce even lighter δ^{30}Si. Moreover, if the average Si isotope composition of the altered oceanic crust was slightly lighter than BSE (e.g., − 0.38‰ vs. − 0.29‰), the residue minerals could also have lighter Si isotope signatures. Therefore, if such a residue was deeply recycled and incorporated into the source of the OIB, it is helpful to explain the heterogeneous Si isotope compositions observed in the OIB.

The melt with heavy δ^{30}Si could also contribute to arc magmas. For example, Poitrasson and Zambardi (2015) found that one arc andesite (JA-2) has relatively heavy δ^{30}Si (− 0.13‰). This arc andesite was possibly derived from melts of subducted oceanic crust. More analyses of Si isotope compositions for arc adakites will be useful for better understanding of such processes.

A conceptual model for Si isotopic fractionation in the subducted oceanic crust and the convective mantle is shown in Fig. 6. During modern subduction, the majority of modern slabs only undergo dehydration. But in a convergent margin with a high geothermal gradient (such as in the Archean or during the subduction of a hot slab), the subducted oceanic crust could also be partially melted at depths of 80–100 km (Poli and Schmidt, 2002; Schmidt et al., 2004; Smith, 2009). As dehydration could release more Pb than U from the slab (e.g., Gill, 1981; Hawkesworth et al., 1991 and references therein), the subducted slabs could build up HIMU signatures with time, which can be preserved from the partial melting process. The melt derived from the subducted crust with heavy Si isotopic signature could be added to the mantle wedge. Furthermore, because the density of the slab residue increases after metamorphism, dehydration, and partial melting, the subducted slabs could sink into the deep mantle even down to the core–mantle boundary where it can remain for ~1 to 2 Gyr (Smith, 2009). The residue of subducted slabs could mix into the source of the mantle plume, producing magmas with HIMU signatures. This scenario is consistent with geodynamic simulations of the convecting mantle (e.g., Ballmer et al., 2017; Deschamps, 2017). As the slab residues might have lighter Si isotopic compositions than the BSE, they could produce HIMU-type OIB with low δ^{30}Si (e.g., − 0.46‰) as observed in Pringle et al. (2016).

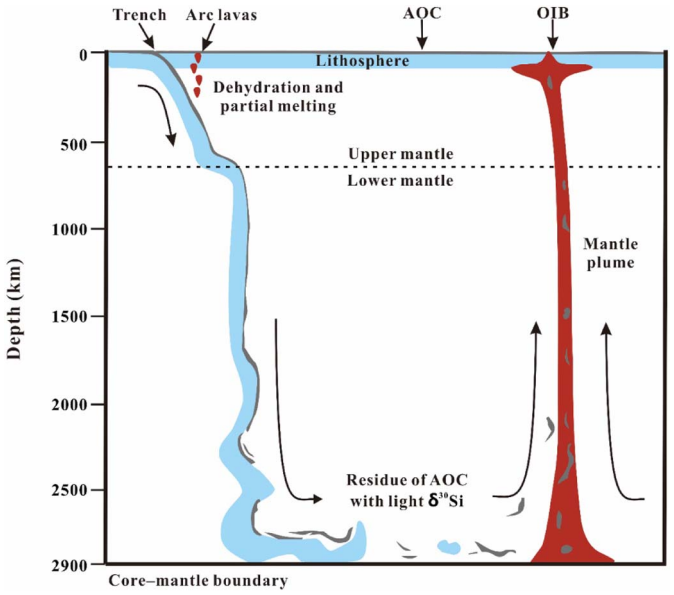

Fig. 6. The conceptual model of Si isotopic fractionation of the subducted oceanic crust in the convective mantle. AOC is altered oceanic crust.

6. Conclusions

The altered oceanic crust recovered from IODP Site 1256, EPR exhibits relatively homogeneous Si isotopic compositions ($\delta^{30}Si = -0.32 \pm 0.06‰$, 2SD), which are in general agreement with the previous estimates of the global fresh MORBs ($-0.27 \pm 0.06‰$, 2SD; Savage et al., 2014). The $\delta^{30}Si$ is not correlated with sample depths, alteration temperatures, and w/r ratios, indicating that both low-temperature seawater alteration and high-temperature hydrothermal alteration did not significantly affect Si isotope compositions at the bulk-rock scale. Therefore, the bulk recycled altered oceanic crust, which is represented by IODP Site 1256, could not be the direct mantle source of the heterogeneous Si isotopes observed in the OIB. However, if the subducted altered oceanic crust is partially melted in the deep mantle, the solid residue of the altered oceanic crust could be enriched in light Si isotopes relative to MORBs, while the melt is enriched in heavy ones. Therefore, the recycling of the isotopically light residue could be helpful to explain the source of some OIBs with light Si isotopic signature.

Supplementary data to this article can be found online at https://doi.org/10.1016/j.chemgeo.2017.12.013.

Acknowledgments

This research was financially supported by MOST of China (2016YFC0600404), the National Science Foundation of China (41503001, 41325011, and 41573017), the Strategic Priority Research Program (B) of the Chinese Academy of Sciences (XDB18000000), and the 111 project. We thank Khadouja Harouaka for helping improve the English of this manuscript. We are grateful to the editorial handling of Dr. Catherine Chauvel and constructive comments from two anonymous reviewers.

References

Abraham, K., Opfergelt, S., Fripiat, F., Cavagna, A.J., De Jong, J., Foley, S.F., André, L., Cardinal, D., 2008. $\delta^{30}Si$ and $\delta^{29}Si$ determinations on USGS BHVO-1 and BHVO-2 reference materials with a new configuration on a Nu plasma multi-collector ICP-MS. Geostand. Geoanal. Res. 32, 193–202.

Alt, J.C., Laverne, C., Coggon, R.M., Teagle, D.A., Banerjee, N.R., Morgan, S., Smith-Duque, C.E., Harris, M., Galli, L., 2010. Subsurface structure of a submarine hydrothermal system in ocean crust formed at the East Pacific Rise, ODP/IODP Site 1256. Geochem. Geophys. Geosyst. 11 (10).

Armytage, R.M.G., Georg, R.B., Savage, P.S., Williams, H.M., Halliday, A.N., 2011. Silicon isotopes in meteorites and planetary core formation. Geochim. Cosmochim. Acta 75 (13), 3662–3676.

Ballmer, M.D., Houser, C., Hernlund, J.W., Wentzcovitch, R.M., Hirose, K., 2017. Persistence of strong silica-enriched domains in the Earth's lower mantle. Nat. Geosci. 10, 236–241.

Basile-Doelsch, I., 2006. Si stable isotopes in the Earth's surface: a review. J. Geochem. Explor. 88 (1), 252–256.

Basile-Doelsch, I., Meunier, J.D., Parron, C., 2005. Another continental pool in the terrestrial silicon cycle. Nature 433 (7024), 399–402.

Bern, C.R., Brzezinski, M.A., Beucher, C., Ziegler, K., Chadwick, O.A., 2010. Weathering, dust, and biocycling effects on soil silicon isotope ratios. Geochim. Cosmochim. Acta 74 (3), 876–889.

Cardinal, D., et al., 2005. Relevance of silicon isotopes to Si-nutrient utilization and Si-source assessment in Antarctic waters. Global Biogeochem. Cycles 19 (2).

Chakrabarti, R., Jacobsen, S.B., 2010. Silicon isotopes in the inner solar system: implications for core formation, solar nebular processes and partial melting. Geochim. Cosmochim. Acta 74 (23), 6921–6933.

Chakrabarti, R., Knoll, A.H., Jacobsen, S.B., Fischer, W.W., 2012. Si isotope variability in Proterozoic cherts. Geochim. Cosmochim. Acta 91, 187–201.

Chan, L.-H., Alt, J.C., Teagle, D.A., 2002. Lithium and lithium isotope profiles through the upper oceanic crust: a study of seawater–basalt exchange at ODP Site 504B and 896A. Earth Planet. Sci. Lett. 201 (1), 187–201.

Chase, C.G., 1981. Oceanic island Pb: two-stage histories and mantle evolution. Earth Planet. Sci. Lett. 52 (2), 277–284.

Chauvel, C., Lewin, E., Carpentier, M., Arndt, N.T., Marini, J.C., 2008. Role of recycled oceanic basalt and sediment in generating the Hf–Nd mantle array. Nat. Geosci. 1 (1), 64–67.

Chemtob, S.M., et al., 2015. Silicon isotope systematics of acidic weathering of fresh basalts, Kilauea Volcano, Hawai'i. Geochim. Cosmochim. Acta 169, 63–81.

Clift, P., Vannucchi, P., 2004. Controls on tectonic accretion versus erosion in subduction zones: implications for the origin and recycling of the continental crust. Rev. Geophys. 42 (2).

Day, J.M.D., Pearson, D.G., Macpherson, C.G., Lowry, D., Carracedo, J.C., 2009. Pyroxenite-rich mantle formed by recycled oceanic lithosphere: oxygen-osmium isotope evidence from Canary Island lavas. Geology 37, 555–558.

De La Rocha, C.L., Brzezinski, M.A., DeNiro, M.J., 2000. A first look at the distribution of the stable isotopes of silicon in natural waters. Geochim. Cosmochim. Acta 64 (14), 2467–2477.

Deines, P., 2002. The carbon isotope geochemistry of mantle xenoliths. Earth Sci. Rev. 58 (3), 247–278.

Delstanche, S., Opfergelt, S., Cardinal, D., Elsass, F., André, L., Delvaux, B., 2009. Silicon isotopic fractionation during adsorption of aqueous monosilicic acid onto iron oxide. Geochim. Cosmochim. Acta 73 (4), 923–934.

Deschamps, F., 2017. Geodynamics: surviving mantle convection. Nat. Geosci. 10, 161–162.

Ding, T., Ma, G.R., Shui, M.X., Wan, D.F., Li, R.H., 2005. Silicon isotope study on rice plants from the Zhejiang province, China. Chem. Geol. 218 (1–2), 41–50.

Dziony, W., Horn, I., Lattard, D., Koepke, J., Steinhoefel, G., Schuessler, J.A., Holtz, F., 2014. In-situ Fe isotope ratio determination in Fe–Ti oxides and sulfides from drilled gabbros and basalt from the IODP Hole 1256D in the eastern equatorial Pacific. Chem. Geol. 363, 101–113.

Eiler, J.M., 2001. Oxygen isotope variations of basaltic lavas and upper mantle rocks. Rev. Mineral. Geochem. 43 (1), 319–364.

Elliott, T., Thomas, A., Jeffcoate, A., Niu, Y., 2006. Lithium isotope evidence for subduction-enriched mantle in the source of mid-ocean-ridge basalts. Nature 443, 565–568.

Fitoussi, C., Bourdon, B., Kleine, T., Oberli, F., Reynolds, B.C., 2009. Si isotope systematics of meteorites and terrestrial peridotites: implications for Mg/Si fractionation in the solar nebula and for Si in the Earth's core. Earth Planet. Sci. Lett. 287 (1–2), 77–85.

France, L., Ildefonse, B., Koepke, J., 2009. Interactions between magma and hydrothermal system in Oman ophiolite and in IODP Hole 1256D: fossilization of a dynamic melt lens at fast spreading ridges. Geochem. Geophys. Geosyst. 10 (10).

Frings, P.J., Clymans, W., Fontorbe, G., Christina, L., Conley, D.J., 2016. The continental Si cycle and its impact on the ocean Si isotope budget. Chem. Geol. 425, 12–36.

Furnes, H., Muehlenbachs, K., Torsvik, T., Thorseth, I.H., Tumyr, O., 2001. Microbial fractionation of carbon isotopes in altered basaltic glass from the Atlantic Ocean, Lau Basin and Costa Rica Rift. Chem. Geol. 173 (4), 313–330.

Gao, Y., Huang, J., Casey, J.F., 2009. Data report: trace element geochemistry of oceanic crust formed at superfast-spreading ridge, Hole 1256D. Proc. IODP 309, 312.

Gao, Y., Vils, F., Cooper, K.M., Banerjee, N., Harris, M., Hoefs, J., Teagle, D.A.H., Casey, J.F., Elliott, T., Laverne, C., Alt, J.C., 2012. Downhole variation of lithium and oxygen isotopic compositions of oceanic crust at East Pacific Rise, ODP Site 1256. Geochem. Geophys. Geosyst. 13 (10).

Georg, R.B., Reynolds, B.C., Frank, M., Halliday, A.N., 2006. New sample preparation techniques for the determination of Si isotopic compositions using MC-ICPMS. Chem. Geol. 235 (1–2), 95–104.

Georg, R.B., Halliday, A.N., Schauble, E.A., Reynolds, B.C., 2007. Silicon in the Earth's core. Nature 447 (7148), 1102–1106.

Gill, J.B., 1981. Geophysical setting of volcanism at convergent plate boundaries. In: Orogenic Andesites and Plate Tectonics. Springer, pp. 44–63.

Graham, D.W., 2002. Noble gas isotope geochemistry of midocean ridge and ocean island basalts: characterization of mantle source reservoirs. Rev. Min. Geochem. 47, 247–317.

Harmon, R.S., Hoefs, J., 1995. Oxygen isotope heterogeneity of the mantle deduced from

global ^{18}O systematics of basalts from different geotectonic settings. Contrib. Mineral. Petrol. 120 (1), 95–114.
Hart, S., Hauri, E., 1992. Mantle plumes and entrainment: isotopic evidence. Science 256 (5056), 517.
Hart, S.R., Blusztajn, J., Dick, H.J., Meyer, P.S., Muehlenbachs, K., 1999. The fingerprint of seawater circulation in a 500-meter section of ocean crust gabbros. Geochim. Cosmochim. Acta 63 (23), 4059–4080.
Hassler, D.R., Shimizu, N., 1998. Osmium isotopic evidence for ancient subcontinental lithospheric mantle beneath the Kerguelen Islands, southern Indian Ocean. Science 280 (5362), 418–421.
Hauri, E.H., Hart, S.R., 1993. Re Os isotope systematics of HIMU and EMII oceanic island basalts from the South Pacific Ocean. Earth Planet. Sci. Lett. 114 (2), 353–371.
Hawkesworth, C., Hergt, J., Ellam, R., Mc Dermott, F., 1991. Element fluxes associated with subduction related magmatism. Philos. Trans. R. Soc. Lond. A Math. Phys. Eng. Sci. 335 (1638), 393–405.
Hofmann, A.W., 1997. Mantle geochemistry: the message from oceanic volcanism. Nature 385, 219–229.
Huang, F., Wu, Z., Huang, S., Wu, F., 2014. First-principles calculations of equilibrium silicon isotope fractionation among mantle minerals. Geochim. Cosmochim. Acta 140, 509–520.
Huang, J., Ke, S., Gao, Y., Xiao, Y., Li, S., 2015. Magnesium isotopic compositions of altered oceanic basalts and gabbros from IODP Site 1256 at the East Pacific Rise. Lithos 231, 53–61.
Huang, J., Liu, S.A., Gao, Y., Xiao, Y., Chen, S., 2016. Copper and zinc isotope systematics of altered oceanic crust at IODP Site 1256 in the eastern equatorial Pacific. J. Geophys. Res. Solid Earth 121 (10), 7086–7100.
Jackson, M.G., Dasgupta, R., 2008. Compositions of HIMU, EM1, and EM2 from global trends between radiogenic isotopes and major elements in ocean island basalts. Earth Planet. Sci. Lett. 276 (1–2), 175–186.
Koepke, J., Christie, D.M., Dziony, W., Holtz, F., Lattard, D., Maclennan, J., Park, S., Scheibner, B., Yamasaki, T., Yamazaki, S., 2008. Petrography of the dyke-gabbro transition at IODP Site 1256 (equatorial Pacific): the evolution of the granoblastic dykes. Geochem. Geophys. Geosyst. 9 (7).
McDonough, W.F., 2003. Compositional model for the Earth's core. In: Holland, H.D., Turekian, K.K. (Eds.), Treatise on Geochemistry. Pergamon, Oxford, pp. 547–568.
Neo, N., Yamazaki, S., Miyashita, S., 2009. Data report: Bulk rock compositions of samples from the IODP Expedition 309/312 sample pool, ODP Hole 1256D. In: Teagle, D.A.H., Alt, J.C., Umino, S., Miyashita, S., Banerjee, N.R., Wilson, D.S. (Eds.), The Expedition. 309. pp. 312.
Nesbitt, H.W., Young, G.M., 1982. Early Proterozoic climates and plate motions inferred from major element chemistry of lutites. Nature 299, 715–717.
Opfergelt, S., de Bournonville, G., Cardinal, D., André, L., Delstanche, S., Delvaux, B., 2009. Impact of soil weathering degree on silicon isotopic fractionation during adsorption onto iron oxides in basaltic ash soils, Cameroon. Geochim. Cosmochim. Acta 73 (24), 7226–7240.
Opfergelt, S., Cardinal, D., André, L., Delvigne, C., Bremond, L., Delvaux, B., 2010. Variations of $\delta^{30}Si$ and Ge/Si with weathering and biogenic input in tropical basaltic ash soils under monoculture. Geochim. Cosmochim. Acta 74 (1), 225–240.
Poitrasson, F., Zambardi, T., 2015. An earth–moon silicon isotope model to track silicic magma origins. Geochim. Cosmochim. Acta 167, 301–312.
Poli, S., Schmidt, M.W., 2002. Petrology of subducted slabs. Annu. Rev. Earth Planet. Sci. 30 (1), 207–235.
Potts, P., 1987. A Handbook of Silicate Rock Analysis. Blackie, London (Search PubMed: 622).
Prentice, A.J., Webb, E.A., 2016. The effect of progressive dissolution on the oxygen and silicon isotope composition of opal-A phytoliths: implications for palaeoenvironmental reconstruction. Palaeogeogr. Palaeoclimatol. Palaeoecol. 453, 42–51.
Pringle, E.A., Moynier, F., Savage, P.S., Jackson, M.G., Moreira, M., Day, J.M., 2016. Silicon isotopes reveal recycled altered oceanic crust in the mantle sources of ocean island basalts. Geochim. Cosmochim. Acta 189, 282–295.
Prytulak, J., Nielsen, S.G., Ionov, D.A., Halliday, A.N., Harvey, J., Kelley, K.A., Niu, Y.L., Peate, D.W., Shimizu, K., Sims, K.W.W., 2013. The stable vanadium isotope composition of the mantle and mafic lavas. Earth Planet. Sci. Lett. 365 (0), 177–189.
Qin, T., Wu, F., Wu, Z., Huang, F., 2016. First-principles calculations of equilibrium fractionation of O and Si isotopes in quartz, albite, anorthite, and zircon. Contrib. Mineral. Petrol. 171 (11), 91.
Robert, F., Chaussidon, M., 2006. A palaeotemperature curve for the Precambrian oceans based on silicon isotopes in cherts. Nature 443 (7114), 969–972.
Rouxel, O., Dobbek, N., Ludden, J., Fouquet, Y., 2003. Iron isotopic fractionation during oceanic crust alteration. Chem. Geol. 202 (1), 155–182.
Roy-Barman, M., Allègre, C.J., 1995. $^{187}Os/^{186}Os$ in oceanic island basalts: tracing oceanic crust recycling in the mantle. Earth Planet. Sci. Lett. 129 (1), 145–161.
Savage, P.S., Georg, R.B., Armytage, R.M.G., Williams, H.M., Halliday, A.N., 2010. Silicon isotope homogeneity in the mantle. Earth Planet. Sci. Lett. 295 (1–2), 139–146.
Savage, P.S., Georg, R.B., Williams, H.M., Burton, K.W., Halliday, A.N., 2011. Silicon isotopic fractionation during magmatic differentiation. Geochim. Cosmochim. Acta 75 (20), 6124–6139.
Savage, P.S., Georg, R.B., Williams, H.M., Halliday, A.N., 2013a. The silicon isotope composition of the upper continental crust. Geochim. Cosmochim. Acta 109 (0), 384–399.
Savage, P.S., Georg, R.B., Williams, H.M., Halliday, A.N., 2013b. Silicon isotopes in granulite xenoliths: insights into isotopic fractionation during igneous processes and the composition of the deep continental crust. Earth Planet. Sci. Lett. 365 (0), 221–231.
Savage, P.S., Armytage, R.M., Georg, R.B., Halliday, A.N., 2014. High temperature silicon isotope geochemistry. Lithos 190, 500–519.
Schmidt, M.W., Vielzeuf, D., Auzanneau, E., 2004. Melting and dissolution of subducting crust at high pressures: the key role of white mica. Earth Planet. Sci. Lett. 228 (1), 65–84.
Smith, A.D., 2009. The fate of subducted oceanic crust and the origin of intraplate volcanism. The lithosphere. Geochem. Geol. Geophys. 123–140.
Sobolev, A.V., Hofmann, A.W., Sobolev, S.V., Nikogosian, I.K., 2005. An olivine-free mantle source of Hawaiian shield basalts. Nature 434 (7033), 590–597.
Spandler, C., Yaxley, G., Green, D.H., Rosenthal, A., 2008. Phase relations and melting of anhydrous K-bearing eclogite from 1200 to 1600 °C and 3 to 5 GPa. J. Petrol. 49 (4), 771–795.
Stracke, A., Hofmann, A.W., Hart, S.R., 2005. FOZO, HIMU, and the rest of the mantle zoo. Geochem. Geophys. Geosyst. 6 (5).
Teagle, D.A.H., Alt, J.C., Umino, S., Miyashita, S., Banerjee, N.R., Wilson, D.S., Expedition 309/312 Scientists, 2006. Superfast Spreading Rate Crust, Proc. Integr. Ocean Drill. Program, 309/312.
Teagle, D.A., Ildefonse, B., Blum, P., 2012. IODP expedition 335: deep sampling in ODP hole 1256D. Sci. Drill. 13, 28–34.
Tomascak, P.B., Langmuir, C.H., le Roux, P.J., Shirey, S.B., 2008. Lithium isotopes in global mid-ocean ridge basalts. Geochim. Cosmochim. Acta 72 (6), 1626–1637.
van den Boorn, S.H., van Bergen, M.J., Nijman, W., Vroon, P.Z., 2007. Dual role of seawater and hydrothermal fluids in Early Archean chert formation: evidence from silicon isotopes. Geology 35 (10), 939–942.
van den Boorn, S., Van Bergen, M., Vroon, P., De Vries, S., Nijman, W., 2010. Silicon isotope and trace element constraints on the origin of ~ 3.5 Ga cherts: implications for Early Archaean marine environments. Geochim. Cosmochim. Acta 74 (3), 1077–1103.
Varela, D.E., Pride, C.J., Brzezinski, M.A., 2004. Biological fractionation of silicon isotopes in Southern Ocean surface waters. Global Biogeochem. Cycles 18 (1).
White, W., Hofmann, A., 1982. Sr and Nd Isotope Geochemistry of Oceanic Basalts and Mantle Evolution.
Wilson, D.S., Teagle, D.A.H., Acton, G.D., et al., 2003. Proc. ODP, Init. Repts., 206: College Station, TX (Ocean Drilling Program). http://dx.doi.org/10.2973/odp.proc.ir.206.2003.
Wilson, D.S., Teagle, D.A., Alt, J.C., Banerjee, N.R., Umino, S., Miyashita, S., Acton, G.D., Anma, R., Barr, S.R., Belghoul, A., Carlut, J., 2006. Drilling to gabbro in intact ocean crust. Science 312 (5776), 1016–1020.
Wu, Z., Huang, F., Huang, S., 2015. Isotope fractionation induced by phase transformation: first-principles investigation for Mg_2SiO_4. Earth Planet. Sci. Lett. 409, 339–347.
Young, E.D., Galy, A., Nagahara, H., 2002. Kinetic and equilibrium mass-dependent isotopic fractionation laws in nature and their geochemical and cosmochemical significance. Geochim. Cosmochim. Acta 66 (6), 1095–1104.
Zambardi, T., Poitrasson, F., 2011. Precise determination of silicon isotopes in silicate rock reference materials by MC-ICP-MS. Geostand. Geoanal. Res. 35 (1), 89–99.
Zambardi, T., Poitrasson, F., Corgne, A., Méheut, M., Quitté, G., Anand, M., 2013. Silicon isotope variations in the inner solar system: implications for planetary formation, differentiation and composition. Geochim. Cosmochim. Acta 121 (0), 67–83.
Zheng, X.-Y., Beard, B.L., Reddy, T.R., Roden, E.E., Johnson, C.M., 2016. Abiologic silicon isotopic fractionation between aqueous Si and Fe(III)–Si gel in simulated Archean seawater: implications for Si isotope records in Precambrian sedimentary rocks. Geochim. Cosmochim. Acta 187, 102–122.
Ziegler, K., Chadwick, O.A., Brzezinski, M.A., Kelly, E.F., 2005. Natural variations of $\delta^{30}Si$ ratios during progressive basalt weathering, Hawaiian Islands. Geochim. Cosmochim. Acta 69 (19), 4597–4610.
Zindler, A., Hart, S., 1986. Chemical geodynamics. Annu. Rev. Earth Planet. Sci. 14, 493–571.